Soft Matter

PAPER

View Article Online
View Journal | View Issue

Cite this: *Soft Matter*, 2024, **20**, 6834

Ionic nanoporous membranes from self-assembled liquid crystalline brush-like imidazolium triblock copolymers†

Iyomali Abeysekera,‡[a] Reuben Bosire, ‡[a] Francis K. Masese,[a] Dennis Ndaya*[ab] and Rajeswari M. Kasi *[ab]

There is a need to generate mechanically and thermally robust ionic nanoporous membranes for separation and fuel cell applications. Herein, we report a general approach to the preparation of ionic nanoporous membranes through custom synthesis, self-assembly, and subsequent chemical manipulations of ionic brush block copolymers. We synthesized polynorbornene-based triblock copolymers containing imidazolium cations balanced by counter anions in the central block, side-chain liquid crystalline units, and sidechain polylactide end blocks. This unique platform comprises: (1) imidazolium/bis(trifluoromethanesulfonyl)imide (TFSI) as the middle block, which has an excellent ion-exchange ability, (2) cyanobiphenyl liquid crystalline end block, a sterically hindered hydrophobic segment, which is chemically stable and immune to hydroxide attack, (3) polylactide brush-like units on the other end block that is easily etched under mild alkaline conditions and (4) a polynorbornene backbone, a lightly crosslinked system that offers mechanical robustness. These membranes retain their morphology before and after backbone crosslinking as well as etching of polylactide sidechains. The ion exchange performance and dimensional stability of these membranes were investigated by water uptake capability and swelling ratio. Moreover, the length of the carbon spacer in the imidazolium/TFSI central block moiety endowed the membrane with improved ionic conductivity. The ionic nanoporous materials are unusual due to their singular thermal, mechanical, alkaline stability and ion transport properties. Applications of these materials include electrochemical actuators, solid-state ionic nanochannel biosensors, and ion-conducting membranes.

Received 16th April 2024,
Accepted 15th July 2024

DOI: 10.1039/d4sm00449c

rsc.li/soft-matter-journal

1. Introduction

Well-designed ion-conducting polymer membranes move charge *via* the transport of ions rather than electrons and function as (poly)electrolytes,[1] electrochemical actuators,[2] and ion exchange membranes for applications in demineralization of salt solutions,[3] desalination,[3] industrial waste treatment,[4] fuel cells,[5] selective separation of different anions by electrodialysis,[6] and high pollution environments.[7] An essential strategy to obtain high ion conductivity and excellent performance includes having densely functionalized ion-conducting groups on a hydrophobic polymer matrix creating ion channels and dimensional stability.[8,9] Tethering the ion exchange on regularly spaced flexible side-chains improves ion conductivity rather than attaching the ion-exchanging head group directly to the polymer backbone.[8,10–12] In principle, lengthening the spacer group should improve the ionic conductivity by supporting the formation of phase-separated morphology.[13,14] This distinct phase separation occurs due to the enthalpy related to the demixing of the hydrophobic polymer backbone with the hydrophilic ionic side chains, typically observed in block copolymer architectures.

Block copolymers containing ion-conducting groups in the main chain and side chains enable the creation of ion conducting membranes or ionic nanochannels (10–100 nm) through control of their microstructures due to clustering of ionic groups and microphase segregation of incompatible domains.[15–17] Furthermore, the composition of the block copolymers, the type and concentration of ionic groups, the presence of spacers, and the morphology and alignment of the ion-conducting domains will impact the thermal properties, mechanical properties, ionic conductivity and ion exchange capacity of these ion-containing block copolymers.[18–20] Also,

[a] *Department of Chemistry, University of Connecticut, Storrs, CT 06269, USA. E-mail: rajeswari.kasi@uconn.edu; Tel: +1-(860)-486-4713*
[b] *Polymer Program, Institute of Material Science, University of Connecticut, Storrs, CT 06269, USA*

† Electronic supplementary information (ESI) available. See DOI: https://doi.org/10.1039/d4sm00449c

‡ These authors contributed equally.

in this architecture, the polymer backbone being protected by the hydrophobic polymer matrix is stable against alkaline media.[21,22]

Another promising approach towards the design of nanochannels with high ion conductivity is to improve ionic mobility. The self-assembly of liquid crystalline polymers is a versatile approach that improves conductivity by creating well-defined and ordered ionic channels.[23–26] Although the incorporation of liquid crystals (LC) to obtain an ordered alignment of ionic clusters is somewhat limited, initial success on designing ion transporting self-assembled soft materials forming 1D, 2D, and 3D ionic pathways has been recently reported.[24,27–29] Thus, the design and structure–property investigation of ion-containing liquid crystalline block copolymers, currently unknown, will be a unique platform for the preparation of ion-conducting materials due to (i) formation of ionic domains from ion-containing groups (imidazolium and pyrimidinium groups), (ii) liquid crystalline ordering, anisotropic ordering and responsive properties and (iii) microphase segregation of block copolymer architecture.

In our previous studies, we used sequential ring opening metathesis polymerization (ROMP) of norbornene monomers to synthesize liquid crystalline brush-like block copolymers (LCBBCs) and explored their phase behavior.[30–32] The advantage of these LCBBCs over conventional liquid crystalline block copolymers is that the introduction of the brush-like side results in tailored meso and micro-structured morphology of these polymers, reduced entanglement and viscosity as well as enhancement of alignment kinetics with or without directed field assemblies. The majority block is composed of polynorbornene bearing side-chain liquid crystalline cyanobiphenyl units, which facilitate the formation of a smectic mesophase.[33–35] The minority block is composed of polynorbornene bearing poly(D,L-lactide) (PLA) brush-like units, which can be selectively etched by hydrolysis under gentle alkaline conditions. The selective removal of PLA blocks results in a functionalized nanoporous surface.[32] The use of the polynorbornene backbone allows the system to be crosslinked and aligned with field-directed assembly, including shear and magnetic alignment, and by using this method, mechanically robust nanoporous membranes could be obtained. Based on this design principle, we recently reported the synthesis and properties of nanoporous membranes from norbornene-backbone-based triblock copolymers containing cyanobiphenyl and polylactide side chain units as end blocks and protected amine or thiol containing monomers in the central block.[32] These amine and thiol groups can ligate to heavy metal ions. The resulting nanoporous membranes are used for heavy metal ion removal applications.[32,36,37]

In principle, the design strategy developed for liquid crystalline nanoporous membranes for metal ion removal can be applied to create a new brush-like liquid crystalline imidazolium functionalized triblock copolymer platform with stable ionic channels and high ion exchange capacity (Fig. 1). Self-assembly within these compression molded films, followed by thiolene crosslinking chemistry of polynorbornene olefinic backbones and mild alkaline selective etching of PLA, presents nanoporous membranes (illustrated in Fig. 1) containing ion-conducting groups with high ion exchange capacity (IEC) and excellent ionic conductivity. The modular platform discussed in this paper is one of its kind: (1) imidazolium/TFSI as the middle block is alkaline stable, has high IEC and ionic conductivy,[38] (2) inclusion of the majority cyanobiphenyl block not only offers natural alignment capabilities but also creates a steric hindrance effect, hence chemically stable and OH-immune conductive nanochannels are produced and (3) the lightly crosslinked hydrophobic polynorbornene system from which PLA side chains can be easily etched under mild alkaline conditions and create alkaline stable ion-conductive nanochannels for potential use in fuel cells and water electrolysis.[37,39–42]

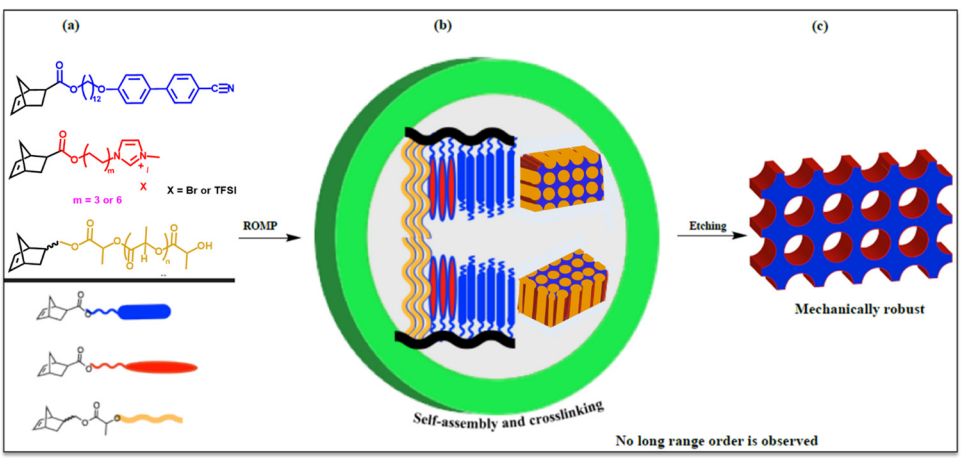

Fig. 1 Schematic illustration of a new nanoporous membrane with high IEC. The design strategy for this system involves (a) sequential block polymerization of three different norbornene monomers (NBCB12 (liquid crystalline unit), NBIm$_m$X (imidazolium unit) and NBPLA (brush-like moiety)), (b) resulting self-assembled triblock copolymer system comprising NBCB12 and NBPLA end blocks and NBIm$_m$X middle block with a crosslinked backbone and (c) etching out PLA to create nanochannels through which ion exchange is realized. The nanoporous membrane produced lacks long-range order and hexagonal arrangements of the pores.

2. Results and discussion

2.1. Synthesis of monomers

The monomers NBCB12[23] and NBPLA2K[32] are synthesized according to previously reported procedures (Fig. S1 and S2, ESI†). New imidazole-functionalized norbornene monomers are synthesized using modified literature procedures and details are provided in Scheme 1.[43]

Briefly, in a dried round-bottomed flask equipped with a magnetic stir bar, 5-norbornene-2- carboxylic acid (3.6 g, 0.026 mol) and 6-bromo-1-hexanol (4 g, 0.022 mol) are dissolved with the help of 30 mL of CH_2Cl_2. Then EDC (6.35 g, 0.033 mol) and a catalytic amount of DMAP and pyridine mixture are added to the reaction mixture stirring at room temperature for 12 h, then the reaction is quenched by adding water (30 mL). The crude product is extracted three times with CH_2Cl_2, and the organic layer is dried with anhydrous $MgSO_4$. Then the organic layer is filtered and concentrated by a rotary evaporator to afford an oily product. The crude product is further purified by column chromatography using hexanes/EtOAc (20 : 1) as the mobile phase and silica gel as the stationary phase to yield a yellow viscous oil, $NB(CH_2)_6Br$ (5.04 g, 76%). ^{1}H NMR (500 MHz, $CDCl_3$): δ 6.17–5.85 (m, 2H), 4.01 (t, 2H), 3.36 (t, 2H), 3.17 (s, 1H), 2.99–2.85 (m, 2H), 2.13–2.22 (m, 3H), 1.92–1.79 (m, 2H), 1.68–1.21 (m, 7H) (Fig. S3, ESI†). The same steps were followed in the synthesis of $NB(CH_2)_{12}Br$, the only slight change was the use of 12-bromo-1-hexanol in place of 6-bromo-1-hexanol.

2.1.1. Synthesis of 5-norbornene-2-carboxylate-1-hexyl-3-methyl-imidazolium. $NB(CH_2)_6Br$ (5.0 g, 0.016 mol) and 1-methylimidazole (1.75 mL, 0.024 mol) are refluxed in acetonitrile for 18 h. After cooling to room temperature, the reaction mixture is concentrated using a rotary evaporator to afford yellow viscous oil and then washed with diethyl ether (3 × 100 mL) to obtain (NBI_6mBr) (4.46 g, 80% yield) (Fig. S3, ESI†). The resulting oil is dissolved in H_2O (100 mL), LiTFSI (4.88 g, 0.017 mol) is added, and the mixture is stirred at room temperature for 12 h.

The yellow oil is extracted with dichloromethane and the organic layer is washed with water and dried over anhydrous $MgSO_4$ to obtain yellow oil, $NBIm_6Fs$ (4.63 g, 75%) (Fig. S4, ESI†). ^{1}H NMR (500 MHz, $CDCl_3$): δ = 8.69 (s, 1H), 7.30 (d, 2H), 6.13–5.86 (m, 2H), 4.11 (t, 2H), 3.96 (t, 2H), 3.71 (s, 3H), 3.15 (s, 1H), 1.84 (m, 2H), 1.82 (m, 3H), 1.58–1.55 (m, 2H), 1.35–1.24 (m, 7H). HRMS: calculated $\{M\}^+$ 303.43, observed 303.20 (Fig. S6, ESI†). The same procedure was followed in the synthesis of the $NBIm_{12}Fs$ monomer, and it was characterized with ^{1}H NMR (Fig. S5, ESI†) and HRMS: calculated $\{M\}^+$ 387.59, observed 387.30 (Fig. S7, ESI†).

2.2. Synthesis of triblock copolymers and preparation of crosslinked ionic membranes

Ring-opening metathesis polymerization (ROMP) of norbornene-functionalized monomers is carried out as shown in Scheme 2. In a typical example, the feed ratio of NBCB12 : $NBIm_{(6\text{ or }12)}X$ (X = Br or Fs): NBPLA2K is 75 : 5 : 20 wt%, which is expected to result in a triblock copolymer with cylinders decorated with imidazolium ions within the polymer

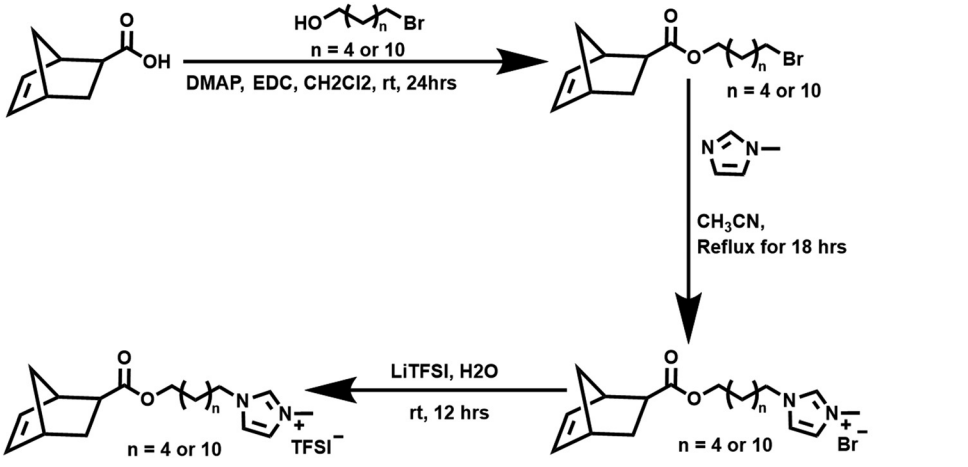

5-norbornene-2-carboxylate-1-hexyl-3-methyl-imidazolium bis((trifluoromethyl)sulfonyl)amide = $NBIm_6Fs$

5-norbornene-2-carboxylate-1-hexyl-3-methyl-imidazolium bromide = $NBIm_6Br$

5-norbornene-2-carboxylate-1-dodecyl-3-methyl-imidazolium bis((trifluoromethyl)sulfonyl)amide = $NBIm_{12}Fs$

5-norbornene-2-carboxylate-1-dodecyl-3-methyl-imidazolium bromide = $NBIm_{12}Br$

Scheme 1 Synthesis of intermediate compounds and monomers, $NB(CH_2)_6Br$), $NB(CH_2)_{12}Br$, 5-norbornene-2-carboxylate-1-hexyl-3-methyl-imidazolium bromide ($NBIm_6Br$), 5-norbornene-2-carboxylate-1-dodecyl-3-methyl-imidazolium bromide ($NBIm_{12}Br$), 5-norbornene-2-carboxylate-1-hexyl-3-methyl-imidazolium bis((trifluoromethyl)sulfonyl)amide ($NBIm_6Fs$), and 5-norbornene-2-carboxylate-1-dodecyl-3-methyl-imidazolium bis((trifluoromethyl)sulfonyl)amide ($NBIm_{12}Fs$).

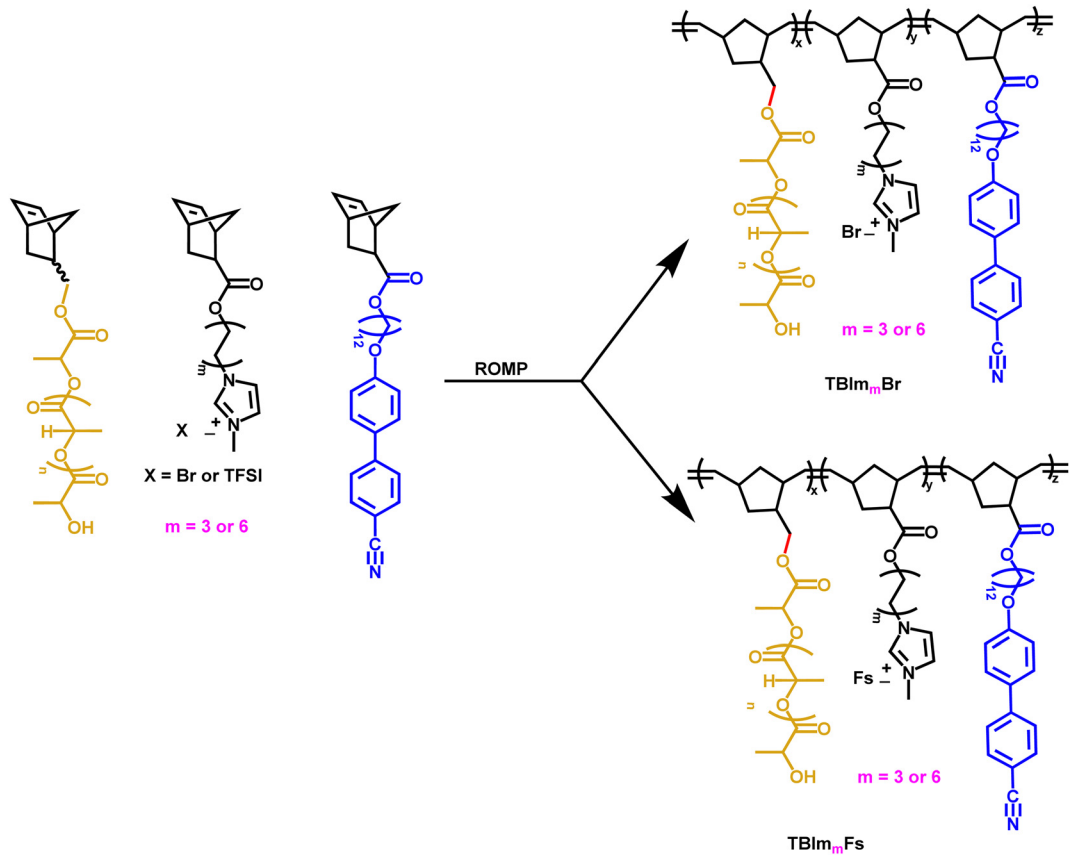

Scheme 2 Synthesis of brush-like triblock copolymers (TBI$_m$Fs) where m = 3 or 6.

matrix.[32] NBCB12 (300 mg, 0.6 mmol) dissolved in 10 mL of CH_2Cl_2 is added to a round-bottomed flask equipped with a magnetic stir bar and a rubber septum and purged with nitrogen for 10 min. In a scintillation vial, modified Grubbs 2nd generation (12.5 mg, 0.018 mmol) is dissolved in CH_2Cl_2 (5 mL) and purged with nitrogen for 10 min. The solution is then added to the round bottom flask containing $NBCB_{12}$ and the reaction is allowed to proceed for 30 min at room temperature. After the completion of first polymerization, the pre-purged CH_2Cl_2 solution containing $NBIm_{(6\text{ or }12)}X$ (X = Fs or Br, 24 mg, 0.05 mmol) is added and stirred for a further 2 hours. Once the completion of second polymerization, the pre-purged CH_2Cl_2 solution containing NBPLA2K (106 mg, 0.05 mmol) is added and stirred for a further 30 minutes. Then, the reaction is terminated by adding excess ethyl vinyl ether (EVE). The resulting polymer is precipitated into a methanol–isopropanol mixture, filtered, and dried overnight in a vacuum oven at room temperature for later use (Table 1).

Table 1 Sample description (E = etched, XL = crosslinked, XLE = crosslinked-etched, subscript indicates the length of the carbon spacer)

Sample description	Labels
Triblock copolymer with Br as counterion	$TBIm_6Br$ $TBIm_6Br$-E $TBIm_6Br$-XL $TBIm_6Br$-XLE
Triblock copolymer with Br as counterion	$TBIm_{12}Br$ $TBIm_{12}Br$-E $TBIm_{12}Br$-XL $TBIm_{12}Br$-XLE
Triblock copolymer with TFSI as counterion	$TBIm_6Fs$ $TBIm_6Fs$-E $TBIm_6Fs$-XL $TBIm_6Fs$-XLE
Triblock copolymer with TFSI as counterion	$TBIm_{12}Fs$ $TBIm_{12}Fs$-E $TBIm_{12}Fs$-XL $TBIm_{12}Fs$-XLE

The successful synthesis of brush-like triblock copolymers is a result of the salient features of ROMP such as its living polymerization, precise molecular weight control, low molecular weight dispersity, and tolerance to an adverse range of functional groups, for example in this case imidazolium groups. The molar composition of the block copolymers is confirmed by ^{1}H NMR spectroscopy. The characteristic proton absorption peaks for the imidazolium ring appear at 10.2 ppm in $NBIm_6Br$ and 8.9 ppm in $NBIm_6Fs$ (Fig. S8–S10, ESI†). When the norbornene monomer is polymerized, the peak broadens but remains at the same position (5.7–6.3 ppm). The successful synthesis of triblock copolymers is confirmed by ^{1}H NMR

Table 2 Molecular composition of triblock copolymers

Copolymer	Feed ratios[a] (determined by ^{1}H NMR wt (%)) NBCB12	NBPLA2K	NBImX (X = Br or TFSI)	Theoretical MW[b] (kg mol^{-1}) (KDa)	GPC, M_n[c] (kg mol^{-1}) ($Đ$)[d]
$TBIm_6Br$	70.0 (67.0)	25.0 (20.5)	5.0 (12.5)	25	20.3 (1.2)
$TBIm_6Fs$	70.0 (69.9)	25.0 (24.2)	5.0 (5.9)	25	21.2 (1.3)
$TBIm_{12}Br$	70.0 (67.5)	25.0 (23.5)	5 (9.0)	25	22.4 (1.2)
$TBIm_{12}Fs$	70.0 (69.7)	25.0 (24.6)	5 (5.7)	25	23.7 (1.1)

[a] The % composition calculated from ^{1}HNMR for $TBIm_{(6\text{ or }12)}Br$ shows a discrepancy from the theoretical value. This could be as a result of the peak used for the case of imidazole at 10.2 ppm for $TBIm_{(6\text{ or }12)}Br$ and 8.9 ppm for $TBIm_{(6\text{ or }12)}Fs$, respectively. The peak is broad due to the surrounding environment composed of Br– or TFSI–. All other peaks overlap with those of NBCB12 and PLA. [b] Theoretical molecular weight of the synthesized triblock copolymers, $TBI_{(6\text{ or }12)}Br$ and $TBI_{(6\text{ or }12)}Fs$. [c] Mn determined by GPC relative to polystyrene standards using the ELSD detector with THF as an eluent. [d] The molecular weight distribution or the polydispersity index ($Đ$).

spectroscopy. Furthermore, the molar compositions of these triblock copolymers are determined, and the related images and results are included in Table 2 and Fig. S8, S9, ESI.† The target theoretical molecular weight of all the triblock copolymers is set at 25 kDa. The GPC results indicate that the terpolymers possess a high degree of polymerization and number average molecular weights of up to ∼23 kg mol^{-1} (Table 3) and a narrow dispersity ($Đ$) of 1.1–1.3.

2.2.1. Crosslinking representative protocol. 200 mg of the triblock copolymer (TBImBr), 5 mg of 2-hydroxy-4′-(2-hydroxyethoxy)-2-methylpropiophenone, and 12 mg of 1,10-decanedithiol are weighed in separate vials covered with aluminum foil. 1 mL of THF is added to the bottles to dissolve the contents and they are mixed thoroughly. The solvent is then evaporated by purging with nitrogen for a few minutes and vacuum dried overnight. A thin film of the sample is produced by compression molding at 82 °C and quenched to room temperature, followed by UV crosslinking for 3 hours resulting in a crosslinked film. The gel fraction of a crosslinked sample in THF is determined to be ∼42%. We followed our previous reported methods to prepare nanoporous membranes decorated with imidazolium ions whose brief details are described in the supporting information (ref. 32).

2.3. Thermal properties

Thermal properties of both triblock copolymers before and after crosslinking and etching are analyzed by thermogravimetric analysis (TGA) and differential scanning calorimetry (DSC), respectively. Both libraries of terpolymers exhibit excellent thermal stability with 5% weight loss from $TBIm_6Fs$ at ∼297 °C, $TBIm_6Br$ at ∼260 °C, $TBIm_{12}$ Br at ∼262 °C, and $TBIm_{12}Fs$ at ∼265 °C (Fig. 2 and Fig. S12, ESI†). Interestingly, the crosslinked and etched terpolymers, $TBIm_6Br$-XLE (∼324 °C), $TBIm_6Fs$-XLE (∼343 °C), $TBIm_{12}Br$-XLE (∼338 °C), and $TBIm_{12}Fs$-XLE (∼349 °C) exhibit much higher thermal stability compared to non-crosslinked ($TBIm_6Br$, $TBIm_6Fs$, $TBIm_{12}Br$, and $TBIm_{12}Fs$), and crosslinked terpolymers, $TBIm_6Br$-XL (∼310 °C), $TBIm_6Fs$-XL (∼316 °C), $TBIm_{12}Br$-XL (∼302 °C), and $TBIm_{12}Fs$-XL (∼311 °C), respectively (Fig. 2 and Fig. S12, ESI†). The thermal stability of the crosslinked and etched terpolymer polymers is promising for membrane applications.

Thermal mesophase transitions of triblock copolymers before and after crosslinking, and PLA etching are determined using DSC. All the samples are heated up to 150 °C to remove thermal history and the first cooling cycle is used to interpret the data. These copolymers exhibit glass transition

Table 3 Average IEC, water uptake, swelling ratio and ionic conductivity values of the synthesized, crosslinked, and etched triblock copolymer thin films

Thin films	Avg IEC (mmol g^{-1})	Water uptake (%)	Swelling ratio (%)	Conductivity (S cm^{-1})
$TBIm_6Br$	0.013 ± 0.001	0.72	0.98	1.41×10^{-5} ± 0.00001
$TBIm_6Br$-E	0.022 ± 0.001	3.23	2.33	2.35×10^{-5} ± 0.00004
$TBIm_6Br$-XL	0.015 ± 0.001	1.32	1.01	1.87×10^{-5} ± 0.00002
$TBIm_6Br$-XLE	0.027 ± 0.003	2.06	1.12	2.32×10^{-5} ± 0.00003
$TBIm_{12}Br$	0.021 ± 0.002	1.49	2.02	2.06×10^{-5} ± 0.00004
$TBIm_{12}Br$-E	0.041 ± 0.003	4.77	5.78	4.15×10^{-5} ± 0.00006
$TBIm_{12}Br$-XL	0.026 ± 0.002	3.84	1.21	2.14×10^{-5} ± 0.00003
$TBIm_{12}Br$-XLE	0.030 ± 0.002	4.14	1.95	3.97×10^{-5} ± 0.00004
$TBIm_6Fs$	0.058 ± 0.004	0.99	1.01	2.34×10^{-5} ± 0.00003
$TBIm_6Fs$-E	0.089 ± 0.005	5.23	10.68	5.57×10^{-5} ± 0.00006
$TBIm_6Fs$-XL	0.076 ± 0.005	2.52	1.25	3.21×10^{-5} ± 0.00004
$TBIm_6Fs$-XLE	0.0870 ± 0.005	5.06	1.13	3.72×10^{-5} ± 0.00003
$TBIm_{12}Fs$	0.061 ± 0.004	3.83	4.97	3.12×10^{-5} ± 0.00005
$TBIm_{12}Fs$-E	0.112 ± 0.006	14.62	17.81	6.02×10^{-5} ± 0.00006
$TBIm_{12}Fs$-XL	0.0656 ± 0.006	8.66	2.98	3.74×10^{-5} ± 0.00004
$TBIm_{12}Fs$-XLE	0.0936 ± 0.0016	12.21	3.62	4.93×10^{-5} ± 0.00005

N.B.: all measurements are measured in triplicates and the average values are recorded. E – etched, XL – crosslinked, XLE – crosslinked and etched/PLA removed.

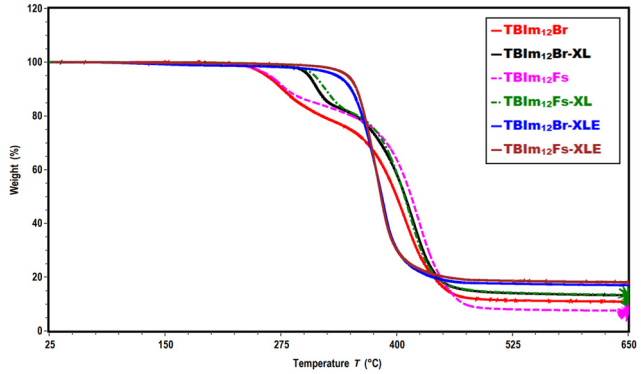

Fig. 2 Thermogravimetric analysis of triblock copolymers before ($TBIm_{12}Br$ and $TBIm_{12}Fs$) and after crosslinking ($TBIm_{12}Br$-XL and $TBIm_{12}Fs$-XL), and after PLA etching ($TBIm_{12}Br$-XLE and $TBIm_{12}Fs$-XLE), respectively.

(T_g) temperature around ~17–22 °C for the non-crosslinked triblocks ($TBIm_6Br$, $TBIm_6Fs$, $TBIm_{12}Br$ and $TBIm_{12}Fs$), and ~25–28 °C for the crosslinked ($TBIm_6Br$-XL, $TBIm_6Fs$-XL, $TBIm_{12}Br$-XL and $TBIm_{12}Fs$-XL), and etched ($TBIm_6Br$-XLE, $TBIm_6Fs$-XLE, $TBIm_{12}Br$-XLE and $TBIm_{12}Fs$-XLE) copolymers, respectively (Fig. 3a and b). The liquid crystalline transition temperature, which is also the liquid crystalline clearing temperature (T_{LC}) for both non-crosslinked and crosslinked triblock copolymers was around ~73–77 °C (Fig. 3a and b), and T_{LC} does not change much after crosslinking and etching (Fig. 3a and b), indicating that post polymerization modifications of crosslinking and etching PLA do not significantly alter the microstructures of these systems.

2.4. Mechanical properties

Dynamic mechanical analysis (DMA) was applied to elucidate the effect of crosslinking on the mechanical performances of the ionic nanoporous membranes. Fig. 3c and d illustrate the tan δ (loss factor/tangent) for the non-crosslinked ($TBIm_6Fs$ and $TBIm_{12}Fs$) copolymers and crosslinked copolymers ($TBIm_6Fs$-XL and $TBIm_{12}Fs$-XL), respectively, as a function of temperature. The tan δ peak maxima values correspond to the thermal properties observed from DSC, the values indicate comparable glass transition temperatures that are consistent with the DSC results. For example, tan δ maxima occurred at ~23 °C for $TBIm_6Fs$, ~31 °C for $TBIm_6Fs$-XL (Fig. 3c), ~22 °C for $TBIm_{12}Fs$, and ~30 °C for $TBIm_{12}Fs$-XL, respectively. The second tan δ peaks observed at ~60–70 °C are associated with liquid crystalline clearing temperature (T_{LC}) of the copolymers and the results are in good agreement with the DSC results (Fig. 3a–d). The crosslinked samples exhibit slightly higher tan δ values, an indication of successful crosslinking, superior energy dissipation from the tougher networks and denser chain

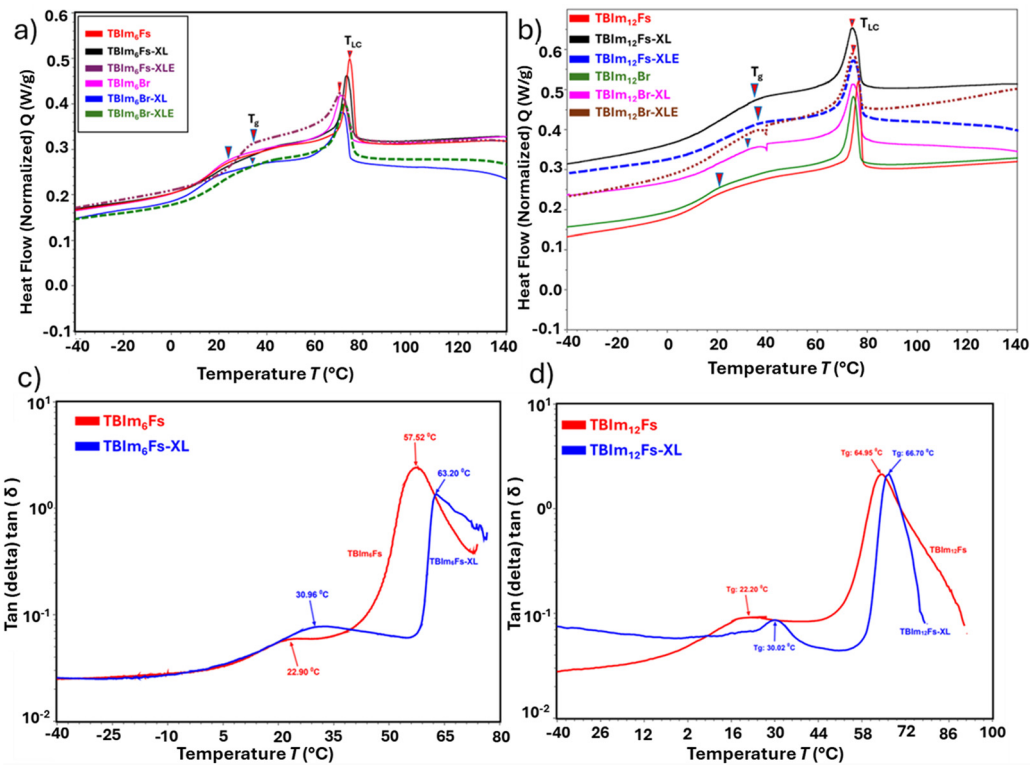

Fig. 3 (a) First cooling cycle DSC thermograms for triblock copolymers before ($TBIm_6Br$ and $TBIm_6Fs$), after crosslinking ($TBIm_6Br$-XL and $TBIm_6Fs$-X), and PLA etching ($TBIm_6Br$-XLE and $TBIm_6Fs$-XLE membranes). (b) First cooling cycle DSC thermograms for triblock copolymers before ($TBIm_{12}Br$ and $TBIm_{12}Fs$), after crosslinking ($TBIm_{12}Br$-XL and $TBIm_{12}Fs$-XL), and PLA etching ($TBIm_{12}Br$-XLE and $TBIm_{12}Fs$-XLE membranes) showing glass transition (T_g) and LC transition temperatures (T_{LC}). (c) and (d) Variation of loss factor, tan δ with temperature for non-crosslinked ($TBIm_{(6\text{ or }12)}Fs$) and crosslinked ($TBIm_{(6\text{ or }12)}Fs$-XL).

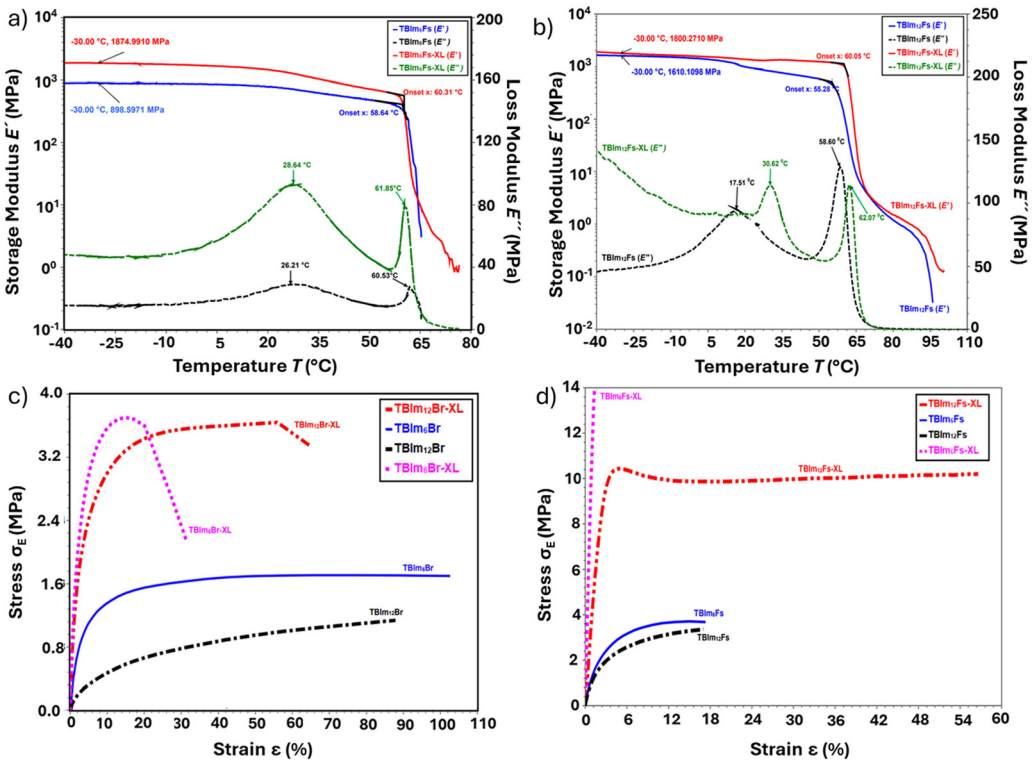

Fig. 4 (a) Variation of storage modulus and loss modulus with temperature for $TBIm_6Fs$-XL and $TBIm_6Fs$ as a control sample. (b) DMA curves for $TBIm_{12}Fs$-XL and $TBIm_{12}Fs$ as control copolymers. (c) Stress–strain curves for $TBIm_6Br$, $TBIm_{12}Br$, $TBIm_6Br$-XL, and $TBIm_{12}Br$-XL. (d) Stress–strain curves for $TBIm_6Fs$, $TBIm_{12}Fs$, $TBIm_6Fs$-XL, and $TBIm_{12}Fs$-XL. The stress–strain behaviors of neat $TBIm_6Br$, $TBIm_{12}Br$, $TBIm_6Fs$, and $TBIm_{12}Fs$ copolymers were compared as control samples.

entanglements in the systems. The DMA storage and loss moduli curves for $TBIm_6Fs$, $TBIm_6Fs$-XL, $TBIm_{12}Fs$, and $TBIm_{12}Fs$-XL are shown in Fig. 4a and b, respectively. Both the storage and loss moduli curve trends depict the thermal transitions (T_g and T_{LC}) for the copolymers. All copolymers exhibited a glass transition region and above it there are rubbery plateaus with crosslinked films having a higher rubbery modulus than non-crosslinked, an indication of successful formation of tough chain networks in the systems. In general, there is a slight decrease in the storage modulus in the T_g region, a sharp decline at >50 °C (T_{LC} region) and sample yielding >75 °C (isotropic region) (Fig. 4a and b). The storage modulus values at low temperatures for $TBIm_6Fs$-XL samples were slightly higher as compared to those of $TBIm_{12}Fs$-XL. The 12-carbon spacer in $TBIm_{12}Fs$-XL could have increased the plasticity in the system that led to flexible chains and elastomeric nature in the systems (Fig. 4c and d). This is demonstrated in the tensile tests (stress–strain curves), and the crosslinked samples had higher toughness and stiffer behaviors as compared to non-crosslinked samples (Fig. 4c and d). Both $TBIm_6Br$-XL and $TBIm_6Fs$-XL were stiffer as compared to $TBIm_{12}Br$-XL and $TBIm_{12}FS$-XL samples (Fig. 4c and d).

As shown in Fig. 4c and d, the non-crosslinked $TBIm_6Br$, and $TBIm_{12}Br$ had a low yield strength of 1.4 MPa and 0.3 MPa, respectively, as compared to crosslinked samples $TBIm_6Br$-XL and $TBIm_{12}Br$-XL which had a yield strength of 3.6 MPa and 3.3 MPa (~157% and 1000% increase in yield strength), respectively. After the introduction of TFSI counterions in both non-crosslinked ($TBIm_6Fs$ and $TBIm_{12}Fs$) and crosslinked samples ($TBIm_6Fs$-XL and $TBIm_{12}Fs$-XL), there was a significant enhancement of the yield strength (Fig. 3c and d). This enhancement can be attributed to additional physical crosslinking from TFSI ion–ion interactions. This in turn reinforces the chemical crosslinking/mechanical properties of the membranes as it can be witnessed in the high yield strength for both $TBIm_6Fs$-XL (13.8 MPa) and $TBIm_{12}Fs$-XL (11.5 MPa) (Fig. 4c and d). Fig. S16 and S17 (ESI†) show the tensile and viscoelastic properties for the etched membranes, $TBIm_{12}Br$-XLE and $TBIm_{12}Fs$-XLE, respectively. As indicated in Fig. S16 (ESI†), the tensile strength for the etched membranes was in the range of 0.25–0.4 MPa, and these values are less than those for the unetched crosslinked membranes. We speculate that the introduction of pores in the nanoporous membranes might have influenced the films' uniformity/thickness, thus affecting their mechanical properties. Tensile properties depend entirely on the uniformity of the films and hence, the stretching capacity in the etched membranes was likely reduced as a result of the size and distribution of the pores in the films leading to low yield strength. However, Fig. S17 (ESI†) clearly shows that even after etching, the targeted nanoporous membranes retain their mechanical integrity at temperatures below and above their glass transition temperatures. The Tan delta curves maxima for

the etched membranes, $TBIm_{12}Fs$-XLE and $TBIm_{12}Br$-XLE occurred at ~25 and ~29 °C and were comparable to those of unetched crosslinked membranes and those observed from DSC.

In general, the crosslinked copolymers with 12 spacer imidazole monomers and $TFSI^-$ ions exhibited a slight decrease in tensile strength, and a slight increase in elongation (large strain break) as compared to both non-crosslinked and crosslinked copolymers with 6 spacer imidazole monomers and Br^- ions, indicating tougher, robust and more flexible nanoporous membranes. Hence, crosslinking leads to a dense, tough, and continuous network which in turn promotes stress transfer and significant mechanical improvement in the systems.[44,45]

The triblock copolymer composition and architecture are designed in such a way that cylindrical morphology in the targeted membranes is obtained and retained. The use of the norbornene backbone is to allow easy thiolene crosslinking chemistries to provide the required rigidity to support the nanopores in these systems. The PLA block is introduced as a sacrificial block by easily etching it using mild basic conditions leaving behind unaltered morphology in the final membrane. Without crosslinking, the stability of the nanopores produced in these systems would be quite limited because of the Laplace pressure. It is therefore necessary to make the system mechanically robust enough to prevent the pore collapse before the nanopores are generated. When crosslinking LC based systems, one should always aim to obtain a mechanically robust system while ensuring that the system retains their morphologies and liquid crystalline properties.

2.5. Microstructural analysis

The crosslinking chemistry and surface chemistry of robust, crosslinked nanoporous membranes (after PLA removal) are confirmed by SEM imaging (Fig. 5). The porous nature of the membrane is revealed by SEM where Fig. 5a and Fig. S13a (ESI†) show unetched samples and Fig. 5b and Fig. S13b (ESI†) show crosslinked etched nanoporous membranes. The pore size for the nanoporous membranes ($TBIm_6Fs$-XLE and $TBIm_{12}Fs$-XLE) from SEM was ~30 ± 3 nm and is in good agreement with the SAXS results and our previous studies (Fig. 7).[32,46] A slight difference exists between the pore size and domain spacing. A similar observation has been noted by Seungwan Cho *et al.* This may be attributed to the enhanced chain mobility in the elevated temperature during etching, leading to a partial collapse of some LC domains during hydrolysis.[46] During crosslinking, the vibrational and stretching bands from the PLA moiety are restricted, thus the peak at 1752 cm^{-1} disappears and the intensity of the peak at 1173 cm^{-1} is reduced relative to other peaks (Fig. 6). The presence of a broad amine peak is indicated by N–H stretching at 3294.3 and 3373.5 cm^{-1}, and N–H bending at 1602 cm^{-1}.[32] The accessibility of functional groups on the surface of nanoporous membranes is revealed by the intensity of these peaks (Fig. S14 and S15, ESI†). The persistence of the C–O stretching ester peak at 1247 cm^{-1} indicates the chemical stability of the triblock terpolymer. The CN stretching vibration observed at 2225 cm^{-1} is attributed to the cyano group from the liquid crystalline moiety.

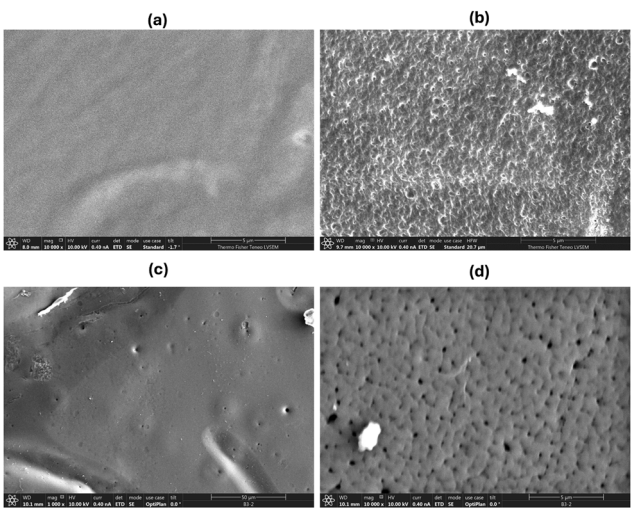

Fig. 5 Comparison of SEM images of gold sputter-coated triblock copolymers (a) before crosslinking ($TBIm_6Br$) and (b) after crosslinking and PLA etching ($TBIm_6Br$-XLE), (c) before crosslinking ($TBIm_6Fs$) and (d) after crosslinking and PLA etching ($TBIm_6Fs$-XLE).

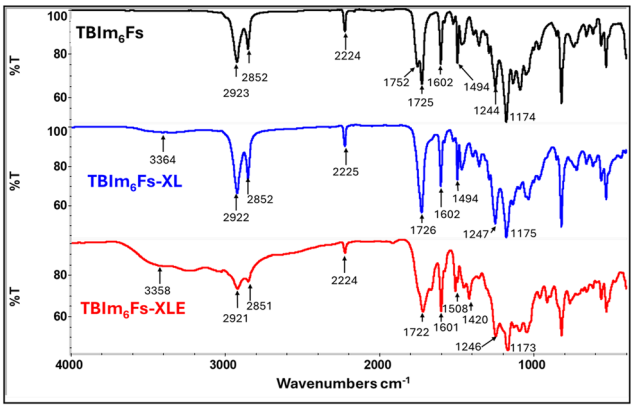

Fig. 6 FTIR spectrum of the $TBIm_6Fs$ triblock copolymer before crosslinking, after crosslinking, and etching of the crosslinked nanoporous samples.

Thus, the ionic nanoporous membrane (triblock copolymer) has several unique features: (1) the imidazolium/TFSI as the middle block is alkaline stable, (2) the cyanobiphenyl block is sterically hindered and hydrophobic and resistant to attack from hydroxide anions that are also used to etch PLA and (3) the lightly crosslinked system is easily etched under alkaline conditions, which only removes PLA but leaves all other chemical constituents intact and creates mechanically stable ion-conductive nanochannels.

2.6. Influence of the membrane microstructure on ion exchange capacity

We previously reported that the norbornene-based liquid crystalline diblock brush copolymer, LC73-PLA27, with composition

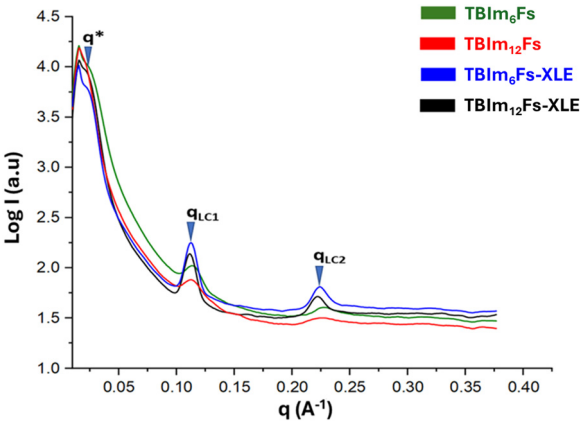

Fig. 7 SAXS profile for the triblock copolymers showing the retention of morphology before and after crosslinking/etching.

comprising NBCB12 of 73 wt% and NBPLA2K of 27 wt% self-assembles into PLA cylinders within majority LC phase from which cylindrical pore nanoporous membranes are derived upon removal of PLA.[36] We also reported the synthesis of triblock copolymers bearing amine and thiol ligands in the central block, which are compression-molded, crosslinked and etched to remove PLA. The nanoporous membrane retains its morphology, an indication that crosslinking does not modify the alignment of the pores. Small angle X-ray scattering analysis of compression molded films of triblock copolymers before ($TBIm_6Fs$ and $TBIm_{12}Fs$) and after crosslinking/etching ($TBIm_6Fs$-XLE and $TBIm_{12}Fs$-XLE, respectively) is shown in Fig. 7.

The triblock copolymers before and after crosslinking and etching show a negligible shift in scattering reflections (q-range positions), which indicates that the microstructure of the liquid crystalline mesophase and the overall morphology of the triblock copolymer are largely unaltered. The SAXS profile of these samples suggests a cylindrical packing of PLA side chains within the smectic layered LC matrix. This is in agreement with the extensive studies that we have previously conducted on these systems and have shown that the full scattering peaks can be observed if the system is aligned under a magnetic field. Using the q^* indicated, the PLA domain decorated on the edges with imidazolium is $\sim$29 nm, and the q_{LC1} indicates that the system is smectic A (SmA) consisting of interdigitated bilayers with a d-spacing of 5.51 nm where q_{LC2} is a higher reflection of q_{LC1}. Additionally, it can be deduced from the scattering pattern observed that there is no long-range hexagonal ordering of the PLA cylinders in the liquid crystalline domains. Furthermore, the porous structure of the membrane may not be continuous through the thickness of the compression-molded triblock copolymer before etching and after etching and crosslinking, respectively. The lack of long-range order of the domain and discontinuous nature of the porous structure while the membrane is mechanically robust and elastomeric are hypothesized to be advantageous when ion exchange studies are carried out.

2.7. Water uptake and swelling ratio

Water uptake (WU) and swelling ratio (SR) are significant parameters in evaluating anion exchange membrane performance. The membrane films are initially soaked in deionized water for 24 h and weighed to obtain the hydrated membrane mass. The films are subsequently dried under a vacuum for 24 h at 80 °C and weighed to obtain their dry weight. Similarly, the swelling ratios are obtained by measuring the length of the films after soaking in deionized water and after vacuum drying. Water uptake is calculated in percent using the following equation:

$$\text{Water uptake} = \frac{\text{mass of hydrated membrane} - \text{mass of dry membrane}}{\text{mass of dry membrane}} \times 100\% \quad (1)$$

Swelling ratio is calculated as follows:

$$\text{Water uptake} = \frac{\text{length of hydrated membrane} - \text{length of dry membrane}}{\text{length of dry membrane}} \times 100\% \quad (2)$$

The water uptake and swelling ratio of the membranes etched in 0.5 M NaOH are observed to increase with an increase in the hydrocarbon chain for both ($TBIm_{(6\text{ or }12)}Br$ and $TBIm_{(6\text{ or }12)}Fs$) polymers (Table 3). This could be attributed to the architectural domains which could possibly allow water to percolate through the polymer matrix. Interestingly, $TBIm_{12}Fs$ films exhibited the highest water uptake and swelling ratios, which are attributed to the network of well-connected bis(trifluoromethanesulfonyl)imide (TFSI) hydrophilic domains improving the films interaction within an aqueous medium. The $TBIm_6Br$ films with hydrophobic polymer domains showed comparatively less water uptake and swelling ratio which are mainly due to lower IEC. Moreover, the water uptake and swelling ratio of the crosslinked/etched films are lower than the etched films but higher than the non-etched films, an indication that crosslinking and etching improved the dimensional stability and the performance of the membranes, respectively. The performance and dimensional stability of the membranes are evaluated based on their water uptake and swelling ratio, thus higher water absorption and less swelling are effective ways to improve conductivity without losing mechanical stability.[47] Notably, the percent swelling ratio values are less compared to those reported in the literature, an indication that these membranes have remarkable dimensional stability endowed by the presence of cyanobiphenyl liquid crystalline end block, a sterically hindered hydrophobic segment, which is chemically

stable and immune to hydroxide attack. The length of carbon spacers was observed to improve the water uptake and swelling ratio.

2.8. Ion exchange capacity (IEC) studies

Ion exchange capacity is a measure of the total ion exchanging sites or functional groups per gram of dry membrane. In liquid crystalline ionic materials, the morphology, domain size (5–10 nm), the counterion on the ion exchange membrane and orientation have a huge impact on ion exchange capacity and/or ionic conductivity.[36] Similarly, block copolymer architecture has been shown to exhibit better ion exchange capacity compared to homopolymers and random copolymers because of the various morphologies that can be achieved through block copolymers which enhances ion transport.[20,48,49] The incorporation of liquid crystalline units within brush-like block copolymers in this study creates defined ionic channels within a liquid crystalline matrix, which ultimately improves ion exchange capacity.[50–52] Furthermore, optimal crosslinking chemistry of the polynorbornene backbone in this study allows for the design of ion exchange membranes with sufficient mechanical integrity as illustrated by the mechanical properties discussed in the previous sections while retaining high ion exchange capacity. This has been a technical challenge in conventional ion exchange membranes that this work addresses.[10,53] The ion exchange capacity (IEC) of the thin films is determined by calibrated potentiometric measurements (Fig. S11, ESI†) and (Table S1, ESI†) and the IEC value is calculated as follows:

$$\mathrm{IEC} = \frac{\text{no. of moles of ions exchanged (mmol)}}{\text{dry weight of the membrane (g)}} \qquad (3)$$

The highest IEC is observed in membranes that are both etched and crosslinked where both membranes $TBIm_{12}Br$-XLE and $TBIm_{12}Fs$-XLE are made up of ~5 wt% of the ion conducting block by composition. It should also be noted that by having flexible methylene spacers between the side chain moieties, the backbone microphase separation is enhanced and this cushions the membrane against mechanical collapse, especially in alkaline environments.[54–57] Li and coworkers have reported an IEC value of 1.85×10^{-3} mol g^{-1} for quaternary ammonium groups grafted onto the norbornene backbone.[58] The observed IEC for this triblock copolymer is comparable to the other reported systems taking into account that the IEC values depend on the content of the ionic ion groups incorporated into the copolymer. Thus, in our present brush-like triblock which contains a small percentage of the ionic block (~5 wt%) in the copolymer composition, the IEC observed, in this case, is significant and indicative of the number of ionic exchange sites available, highlighting the potential for use as ion exchange membranes or ion-conducting membranes.[59–61]

The alkaline stability of the nanoporous ionic membrane is promoted by the presence of π-electrons from imidazolium and cyanobiphenyl groups.[62,63] The chemical stability is further enhanced by the norbornene backbone, the alkyl spacer between the norbornene backbone and imidazolium group.[64,65] Our system is particularly intriguing due to the well-defined polymer morphology supporting both ion conductivity and membrane stability. Additionally, the presence of discontinuous pores facilitates the performance of the membrane *via* the formation of ion channels and increasing surface area for ion exchange. The IEC and ionic conductivity performance of the thin films immersed in an alkaline solution (0.5 M NaOH) for etching compared to the unetched films indicates that these films exhibit alkaline stability behavior.[66] Mckeown, Guiver and Xu *et al.* reported that microporous copolymer ionomer based AEM shows high ion conductivity suggesting that the microporosity of the charged copolymer matrix facilitates the ion transport.[67] Zhang *et al.* reported that semi-flexible poly(aryl ether sulfone) containing flexible aliphatic side-chains with imidazolium cations at the end shows high hydroxide conductivity (93 mS cm^{-1} at 60 °C), highlighting the fact that the introduction of flexible side chains increases the mobility leading to better hydrophilic/hydrophobic microphase separation.[68] In summary, while several strategies have been developed over the years to achieve high conductivity and acceptable alkaline stability, our work presents a novel approach to the molecular engineering of mechanically, thermally and alkaline stable, nanoporous membranes with unusually high IEC despite comprising 5 wt% of the ion exchange moiety in the polymer architecture.

2.9. Ionic conductivity of thin films

The ionic conductivity of the thin films comprising only 5 wt% of the ion exchange moiety in the polymer architecture is evaluated using the Osilla Four Point Probe. The conductivity of the terpolymer with Br as the counterion increases from 1.41×10^{-5} to 2.32×10^{-5}. On the other hand, the conductivity of the terpolymer, $TBIm_6Fs$ with TFSI as the counterion increases from 2.34×10^{-5} to 3.72×10^{-5} (Table 3). Etching thin films helps create anchoring points for ions in the polymer matrix,[69] while crosslinking helps to introduce branched structures that provide a certain free volume to help build ion channels with lower transmission resistance.[70,71] When compared to the terpolymers with Br as counterions, the terpolymers with TFSI as counterions showed higher ionic conductivity (σ) (Table 3). This could be attributed to the excellent ion-exchange ability of the imidazolium/TFSI central block moiety and its hydrophilicity, which improves the membrane interaction with water. Notably, ionic conductivity also increases with the increase in carbon spacer groups due to improved hydroxyl interactions with the polymers' functional groups due to bond flexibility, improving the local mobility of cationic groups.[72]

3. Conclusions

We describe the synthesis, properties, and high ion exchange capacity of a novel brush like liquid crystalline imidazolium functionalized triblock copolymer platform (as high IEC capacity nanoporous membranes) by ring-opening metathesis polymerization for potential use as an anion exchange membrane

for fuel cells and water electrolysis applications. The majority block contains a side-chain LC block that provides some degree of order that may be further enhanced due to their ability to align under the applied external field, and the PLA brush-like block allows the formation of nanopores decorated with ion-containing imidazolium cations counterbalanced by anions. The triblock copolymers and subsequent crosslinked ion-conducting nanoporous membranes are thermally stable with some nanoporous membranes such as $TBIm_{12}Fs$-XLE having degradation temperatures at 5% weight loss, T_d, as high as 349 °C, well above the 150 °C, which is the typical operating temperature for fuel cells and water electrolysis applications. These crosslinked membranes are mechanically robust as has been illustrated by the detailed analysis of mechanical properties. The morphology of the nanoporous membranes was established by SEM and SAXS, and the size of the pores is determined to be ~32 nm, with the domain spacing ranging from ~28 to 30 nm. The morphological studies indicate that the nanoporous membrane may not be continuous throughout the thickness of the pores and lack long-range order. However, for optimal IEC and ionic conductivity, these morphological characteristics are highly desirable for these applications. IEC is determined using potentiometry, and the highest IEC is observed for films that are both crosslinked and etched, which suggests that the formation of nanopores facilitates ion conductivity and is not impeded by lack of long-range order. Ongoing studies are focused on methods to optimize long-range order using aligning capabilities of the cyanobiphenyl units as well as the construction of continuous nanopores and their impact on IEC and ionic conductivity of these new materials for AEM applications.

Data availability

All of the data reported in this manuscript are available in tables and figures both in the main manuscript as well as the ESI.†

Conflicts of interest

There are no conflicts of interest to declare.

Acknowledgements

This work was supported by the NSF under grants DMR-1507045 and CMMI-1246804. The central instrumentation facilities at the Institute of Materials Science and Chemistry Department at UConn are acknowledged.

References

1 D. Kitto and J. Kamcev, The need for ion-exchange membranes with high charge densities, *J. Membr. Sci.*, 2023, 121608.
2 F. Braz Ribeiro, B. Ni, G. T. Nguyen, E. Cattan, A. S. Shaplov, F. Vidal and C. Plesse, Highly Stretchable and Ionically Conductive Membranes with Semi-Interpenetrating Network Architecture for Truly All-Solid-State Microactuators and Microsensors, *Adv. Mater. Interfaces*, 2023, **10**(10), 2202381.
3 H. Chen, X. Liu, D. Gong, C. Zhu, G. Liu, J. Fan, P. Wu, Z. Li, Y. Pan and G. Shi, Ultrahigh-water-flux desalination on graphdiyne membranes, *Nat. Water*, 2023, **1**(9), 800–807.
4 A. Sahu, R. Dosi, C. Kwiatkowski, S. Schmal and J. C. Poler, Advanced polymeric nanocomposite membranes for water and wastewater treatment: a comprehensive review, *Polymers*, 2023, **15**(3), 540.
5 L. S. Kuznetsova, V. A. Arlyapov, Y. V. Plekhanova, S. E. Tarasov, A. S. Kharkova, E. A. Saverina and A. N. Reshetilov, Conductive Polymers and Their Nanocomposites: Application Features in Biosensors and Biofuel Cells, *Polymers*, 2023, **15**(18), 3783.
6 H. Fan, Y. Xu, F. Zhao, Q.-B. Chen, D. Wang and J. Wang, A novel porous asymmetric cation exchange membrane with thin selective layer for efficient electrodialysis desalination, *Chem. Eng. J.*, 2023, **472**, 144856.
7 Y. Cheng, C. Xia, H. A. Garalleh, M. Garaleh, N. T. L. Chi and K. Brindhadevi, A review on optimistic development of polymeric nanocomposite membrane on environmental remediation, *Chemosphere*, 2023, **315**, 137706.
8 T. L. Price, U. H. Choi, D. V. Schoonover, M. Arunachalam, R. Xie, S. Lyle, R. H. Colby and H. W. Gibson, Ion Conducting ROMP Monomers Based on (Oxa)norbornenes with Pendant Imidazolium Salts Connected via Oligo(oxyethylene) Units and with Oligo(ethyleneoxy) Terminal Moieties, *Macromolecules*, 2019, **52**(4), 1371–1388.
9 S. Zheng, S. Zhao, H. Tan, R. Wang, M. Zhai, H. Zhang, H. Qin and H. Tang, Construction of reliable ion-conducting channels based on the perfluorinated anion-exchange membrane for high-performance pure-water-fed electrolysis, *Adv. Compos. Hybrid Mater.*, 2023, **6**(3), 89.
10 J. Thomas, M. E. Thomas, S. Thomas, A. Schechter and F. Grynszpan, A perspective into recent progress on the tailored cationic group-based polymeric anion exchange membranes intended for electrochemical energy applications, *Mater. Today Chem.*, 2024, **35**, 101866.
11 Y. Xie, S. Li, J. Pang and Z. Jiang, Micro-block poly (arylene ether sulfone) s with densely quaternized units for anion exchange membranes: Effects of benzyl N-methylpiperidinium and benzyl trimethyl ammonium cations, *J. Membr. Sci.*, 2023, **669**, 121333.
12 W. You, K. J. Noonan and G. W. Coates, Alkaline-stable anion exchange membranes: A review of synthetic approaches, *Prog. Polym. Sci.*, 2020, **100**, 101177.
13 T. Wang, Y. Zhao, S. Wang, S. Cheng, S. Yang, H. Wei and Y. Ding, Towards high alkaline stability and fuel cell performance in anion exchange membranes via backbone–cation alkylene spacer tuning for quaternized poly (biphenylene alkylene)s, *J. Power Sources*, 2023, **557**, 232590.
14 Y. Zhao, Y. Yang, S. Wang, T. Wang, C. Liu, S. Cheng, H. Wei and Y. Ding, Rational design protocols to tune the

morphology and conductivity of poly (arylene alkylene)-based anion exchange membranes, *J. Membr. Sci.*, 2023, **688**, 122132.

15 J. Li, C. Liu, J. Ge, W. Xing and J. Zhu, Challenges and Strategies of Anion Exchange Membranes in Hydrogen-electricity Energy Conversion Devices, *Chem. – Eur. J.*, 2023, **29**(26), e202203173.

16 L. Yang, C. Fan, H. Gao and J. L. Schaefer, Developing Alkaline Exchange Membranes Using Multisegmented Block Copolymers from Friedel–Crafts Hydroxyalkylation Polycondensation, *Macromolecules*, 2024, **57**(3), 1195–1206.

17 L. X. Sun, W. W. Gou, X. L. Gao, Q. Yang, Q. G. Zhang, A. M. Zhu and Q. L. Liu, End-group crosslinked hexafluorobenzene contained anion exchange membranes, *Int. J. Hydrogen Energy*, 2021, **46**(80), 39921–39931.

18 M. Gopinadhan, Y. Choo, K. Kawabata, G. Kaufman, X. Feng, X. Di, Y. Rokhlenko, L. H. Mahajan, D. Ndaya, R. M. Kasi and C. O. Osuji, Controlling orientational order in block copolymers using low-intensity magnetic fields, *Proc. Natl. Acad. Sci. U. S. A.*, 2017, **114**(45), E9437.

19 H. J. Kim, B. Chen, Z. Suo and R. C. Hayward, Ionoelastomer junctions between polymer networks of fixed anions and cations, *Science*, 2020, **367**(6479), 773.

20 X. Li, K. Yang, Z. Wang, Y. Chen, Y. Li, J. Guo, J. Zheng, S. Li and S. Zhang, Chain architecture dependence of morphology and water transport in poly (fluorene alkylene)-based anion-exchange membranes, *Macromolecules*, 2022, **55**(23), 10607–10617.

21 X. Chen, Y. Zhan, J. Tang, X. Yang, A. Sun, B. Lin, F. Zhu, H. Jia and X. Lei, Advances in high performance anion exchange membranes: molecular design, preparation methods, and ion transport dynamics, *J. Environ. Chem. Eng.*, 2023, 110749.

22 W. Song, X. Zhang, C. Yang, Z. Yang, L. Wu, X. Ge and T. Xu, Alkaline membranes toward electrochemical energy devices: recent development and future perspectives, *ACS Cent. Sci.*, 2023, **9**(8), 1538–1557.

23 P. Deshmukh, M. Gopinadhan, Y. Choo, S.-K. Ahn, P. W. Majewski, S. Y. Yoon, O. Bakajin, M. Elimelech, C. O. Osuji and R. M. Kasi, Molecular Design of Liquid Crystalline Brush-Like Block Copolymers for Magnetic Field Directed Self-Assembly: A Platform for Functional Materials, *ACS Macro Lett.*, 2014, **3**(5), 462–466.

24 Z. Zhu, D. Wang, Y. Tian and L. Jiang, Ion/Molecule Transportation in Nanopores and Nanochannels: From Critical Principles to Diverse Functions, *J. Am. Chem. Soc.*, 2019, **141**(22), 8658–8669.

25 J. Kloos, N. Joosten, A. Schenning and K. Nijmeijer, Self-assembling liquid crystals as building blocks to design nanoporous membranes suitable for molecular separations, *J. Membr. Sci.*, 2021, **620**, 118849.

26 S. J. Lugger, S. J. Houben, Y. Foelen, M. G. Debije, A. P. Schenning and D. J. Mulder, Hydrogen-bonded supramolecular liquid crystal polymers: smart materials with stimuli-responsive, self-healing, and recyclable properties, *Chem. Rev.*, 2021, **122**(5), 4946–4975.

27 H. K. Bisoyi and Q. Li, Liquid crystals: versatile self-organized smart soft materials, *Chem. Rev.*, 2021, **122**(5), 4887–4926.

28 J. Uchida, B. Soberats, M. Gupta and T. Kato, Advanced functional liquid crystals, *Adv. Mater.*, 2022, **34**(23), 2109063.

29 C.-H. Wu, W. Meng, K. Iakoubovskii and M. Yoshio, Photocured liquid-crystalline polymer electrolytes with 3D ion transport pathways for electromechanical actuators, *ACS Appl. Mater. Interfaces*, 2023, **15**(3), 4495–4504.

30 D. Ndaya, R. Bosire and R. M. Kasi, Spherical photonic nanostructures from high molecular weight liquid crystalline brushlike block copolymers, *ACS Appl. Polym. Mater.*, 2020, **2**(12), 5511–5520.

31 D. Ndaya, R. Bosire, S. Vaidya and R. M. Kasi, Molecular engineering of stimuli-responsive, functional, side-chain liquid crystalline copolymers: Synthesis, properties and applications, *Polym. Chem.*, 2020, **11**(37), 5937–5954.

32 D. Ndaya, R. Bosire, L. Mahajan, S. Huh and R. Kasi, Synthesis of ordered, functional, robust nanoporous membranes from liquid crystalline brush-like triblock copolymers, *Polym. Chem.*, 2018, **9**(12), 1404–1411.

33 M. Gopinadhan, P. Deshmukh, Y. Choo, P. W. Majewski, O. Bakajin, M. Elimelech, R. M. Kasi and C. O. Osuji, Thermally Switchable Aligned Nanopores by Magnetic-Field Directed Self-Assembly of Block Copolymers, *Adv. Mater.*, 2014, **26**(30), 5148–5154.

34 R. Bosire, D. Ndaya and R. M. Kasi, Cholesteric mesophase based 1D photonic materials from self-assembly of liquid crystalline block and random terpolymers containing chromonic molecules, *RSC Adv.*, 2021, **11**(24), 14615–14623.

35 C. Lee, D. Ndaya, R. Bosire, N. K. Kim, R. M. Kasi and C. O. Osuji, Fast photoswitchable order–disorder transitions in liquid-crystalline block co-oligomers, *J. Am. Chem. Soc.*, 2021, **144**(1), 390–399.

36 Y. Choo, L. H. Mahajan, M. Gopinadhan, D. Ndaya, P. Deshmukh, R. M. Kasi and C. O. Osuji, Phase Behavior of Polylactide-Based Liquid Crystalline Brushlike Block Copolymers, *Macromolecules*, 2015, **48**(22), 8315–8322.

37 L. Mahajan, D. Ndaya, P. Deshmukh and R. Kasi, New Stimuli-Response Liquid Crystalline Polymer Architectures, *Liq. Cryst. Polym.*, 2020, 479–492.

38 K. Matsumoto, T. Yano, S. Date, Y. Odahara and S. Narimura, Synthesis of imidazolium-based poly (ionic liquid) s and their application to ion-exchange materials, *Polym. Bull.*, 2021, **78**, 5165–5180.

39 M. Mandal, G. Huang and P. A. Kohl, Anionic multiblock copolymer membrane based on vinyl addition polymerization of norbornenes: Applications in anion-exchange membrane fuel cells, *J. Membr. Sci.*, 2019, **570–571**, 394–402.

40 P. Xiong, L. Zhang, Y. Chen, S. Peng and G. Yu, A chemistry and microstructure perspective on ion-conducting membranes for redox flow batteries, *Angew. Chem., Int. Ed.*, 2021, **60**(47), 24770–24798.

41 M. Lehmann, D. Leonard, J. Zheng, L. He, X. Tang, X. C. Chen, K. H. Lim, S. Maurya, Y. S. Kim and T. Saito,

Quaternized Polynorbornene Random Copolymers for Fuel Cell Devices, *ACS Appl. Energy Mater.*, 2023, **6**(3), 1822–1833.
42 M. Hren, M. Božič, D. Fakin, K. S. Kleinschek and S. Gorgieva, Alkaline membrane fuel cells: anion exchange membranes and fuels, *Sustainable Energy Fuels*, 2021, **5**(3), 604–637.
43 J. Wang, X. He, H. Zhu and D. Chen, Preparation of a ROMP-type imidazolium-functionalized norbornene ionic liquid block copolymer and the electrochemical property for lithium-ion batteries polyelectrolyte membranes, *RSC Adv.*, 2015, **5**(54), 43581–43588.
44 F. K. Masese, P. K. Njenga, D. M. Ndaya and R. M. Kasi, Recent Advances and Opportunities for Cellulose Nanocrystal-Based Liquid Crystalline Polymer Hybrids and Composite Materials, *Macromolecules*, 2023, **56**(17), 6567–6588.
45 B. Lin, F. Xu, F. Chu, Y. Ren, J. Ding and F. Yan, Bis-imidazolium based poly(phenylene oxide) anion exchange membranes for fuel cells: the effect of cross-linking, *J. Mater. Chem. A*, 2019, **7**(21), 13275–13283.
46 S. Cho, J. Son, I. Kim, H. Ahn, H.-S. Jang, S. H. Joo, K. H. Park, E. Lee, Y. Kim and S.-K. Ahn, Asymmetric polystyrene-polylactide bottlebrush random copolymers: Synthesis, self-assembly and nanoporous structures, *Polymer*, 2019, **175**, 49–56.
47 I. Arunkumar, A. R. Kim, S. H. Lee and D. J. Yoo, Enhanced fumion nanocomposite membranes embedded with graphene oxide as a promising anion exchange membrane for fuel cell application, *Int. J. Hydrogen Energy*, 2022, **52**(10), 139–153.
48 I. Jeong, K. Min, H. Kim, S. Y. Nam and T.-H. Kim, Poly (dibenzofuran-p-terphenyl piperidinium)-based anion exchange membranes with enhanced phase separation for water electrolysis, *J. Membr. Sci.*, 2023, **687**, 122079.
49 B. Xue, W. Cui, S. Zhou, Q. Zhang, J. Zheng, S. Li and S. Zhang, Facile preparation of highly alkaline stable poly (arylene–imidazolium) anion exchange membranes through an ionized monomer strategy, *Macromolecules*, 2021, **54**(5), 2202–2212.
50 K. V. Axenov and S. Laschat, Thermotropic ionic liquid crystals, *Materials*, 2011, **4**(1), 206–259.
51 K. Hoshino, M. Yoshio, T. Mukai, K. Kishimoto, H. Ohno and T. Kato, Nanostructured ion-conductive films: Layered assembly of a side-chain liquid-crystalline polymer with an imidazolium ionic moiety, *J. Polym. Sci., Part A: Polym. Chem.*, 2003, **41**(22), 3486–3492.
52 T. Kato, M. Gupta, D. Yamaguchi, K. P. Gan and M. Nakayama, Supramolecular association and nanostructure formation of liquid crystals and polymers for new functional materials, *Bull. Chem. Soc. Jpn.*, 2021, **94**(1), 357–376.
53 H. Chen, R. Tao, K. T. Bang, M. Shao and Y. Kim, Anion exchange membranes for fuel cells: state-of-the-art and perspectives, *Adv. Energy Mater.*, 2022, **12**(28), 2200934.
54 J. Ran, L. Wu, Y. He, Z. Yang, Y. Wang, C. Jiang, L. Ge, E. Bakangura and T. Xu, Ion exchange membranes: New developments and applications, *J. Membr. Sci.*, 2017, **522**, 267–291.
55 D.-Y. Park, P. A. Kohl and H. W. Beckham, Anion-Conductive Multiblock Aromatic Copolymer Membranes: Structure–Property Relationships, *J. Phys. Chem. C*, 2013, **117**(30), 15468–15477.
56 A. D. Mohanty, C. Y. Ryu, Y. S. Kim and C. Bae, Stable Elastomeric Anion Exchange Membranes Based on Quaternary Ammonium-Tethered Polystyrene-*b*-poly(ethylene-*co*-butylene)-*b*-polystyrene Triblock Copolymers, *Macromolecules*, 2015, **48**(19), 7085–7095.
57 A. D. Mohanty, S. E. Tignor, J. A. Krause, Y.-K. Choe and C. Bae, Systematic Alkaline Stability Study of Polymer Backbones for Anion Exchange Membrane Applications, *Macromolecules*, 2016, **49**(9), 3361–3372.
58 S. Li, H. Zhang, K. Wang, F. Yang, Y. Han, Y. Sun, J. Pang and Z. Jiang, Anion conductive piperidinium based poly (ether sulfone): Synthesis, properties and cell performance, *J. Membr. Sci.*, 2020, **594**, 117471.
59 D. Xu, J. Guo and F. Yan, Porous ionic polymers: Design, synthesis, and applications, *Prog. Polym. Sci.*, 2018, **79**, 121–143.
60 I. Salmeron-Sanchez, J. Asenjo-Pascual, J. R. Avilés-Moreno, J. Pérez-Flores, P. Mauleón and P. Ocón, Chemical physics insight of PPy-based modified ion exchange membranes: A fundamental approach, *J. Membr. Sci.*, 2022, **643**, 120020.
61 J. Zhang, W. Yu, X. Liang, K. Zhang, H. Wang, X. Ge, C. Wei, W. Song, Z. Ge and L. Wu, Flexible bis-piperidinium side chains construct highly conductive and robust anion-exchange membranes, *ACS Appl. Energy Mater.*, 2021, **4**(9), 9701–9711.
62 R. Mondal, S. Pal and U. Chatterjee, Alkylated imidazole moieties in a cross-linked anion exchange membrane facilitate acid recovery with high purity, *ACS Appl. Polym. Mater.*, 2021, **3**(3), 1544–1554.
63 Y. Zhai, C. Li and L. Gao, Degradable block copolymer-derived nanoporous membranes and their applications, *Giant*, 2023, 100183.
64 X. He, C. Cheng, S. Huang, F. Zhang, Y. Duan, C. Zhu, Y. Guo, K. Wang and D. Chen, Alkaline anion exchange membranes with imidazolium-terminated flexible side-chain cross-linked topological structure based on ROMP-type norbornene copolymers, *Polymer*, 2020, **195**, 122412.
65 C. Cheng, X. He, S. Huang, F. Zhang, Y. Guo, Y. Wen, B. Wu and D. Chen, Novel self-cross-linked multi-imidazolium cations long flexible side chains triblock copolymer anion exchange membrane based on ROMP-type polybenzonorbornadiene, *Int. J. Hydrogen Energy*, 2020, **45**(38), 19676–19690.
66 B. Lin, F. Xu, F. Chu, Y. Ren, J. Ding and F. Yan, Bis-imidazolium based poly (phenylene oxide) anion exchange membranes for fuel cells: the effect of cross-linking, *J. Mater. Chem. A*, 2019, **7**(21), 13275–13283.
67 Z. Yang, R. Guo, R. Malpass-Evans, M. Carta, N. B. McKeown, M. D. Guiver, L. Wu and T. Xu, Highly conductive anion-exchange membranes from microporous

Tröger's base polymers, *Angew. Chem.*, 2016, **128**(38), 11671–11674.

68 X. Zhang, S. Li, P. Chen, J. Fang, Q. Shi, Q. Weng, X. Luo, X. Chen and Z. An, Imidazolium functionalized block copolymer anion exchange membrane with enhanced hydroxide conductivity and alkaline stability via tailoring side chains, *Int. J. Hydrogen Energy*, 2018, **43**(7), 3716–3730.

69 Y. B. Yang, W. Chai, L. Zhang, J. Wang and J. You, A mini-review of polymeric porous membranes with vertically penetrative pores, *J. Polym. Sci.*, 2024, **62**(3), 492–507.

70 X. Su, S. Nan, W. Wei, S. Xu and R. He, Highly conductive and robustly stable anion exchange membranes with a star-branched crosslinking structure, *J. Membr. Sci.*, 2023, **683**, 121843.

71 L. Bai, L. Ma, L. Li, A. Zhang, X. Yan, F. Zhang and G. He, Branched, side-chain grafted polyarylpiperidine anion exchange membranes for fuel cell application, *ACS Appl. Energy Mater.*, 2021, **4**(7), 6957–6967.

72 S. Kadulkar, Z. W. Brotherton, A. L. Lynch, G. Pohlman, Z. Zhang, R. Torres, A. Manthiram, N. A. Lynd, T. M. Truskett and V. Ganesan, The Importance of Morphology on Ion Transport in Single-Ion, Comb-Branched Copolymer Electrolytes: Experiments and Simulations, *Macromolecules*, 2023, **56**(7), 2790–2800.